

Tailoring optical response in nanostructured bilayers: Effects of surface roughness and layer thickness on NbN/Nb and TiN/Ti

J.A. Polito-Lucas, F.J. Flores-Ruiz, V. Garcia-Vazquez, A.L. González

Numerical calculations were performed on NbN/Nb and TiN/Ti nanostructured bilayers. Discrete dipole approximation implemented in the DDSCAT code was utilized. In order to design a TUC (Target Unit Cell) with realistic surface-roughness pattern, Atomic Force Microscope images of 100 ± 10 nm Nb thin films were used. The optical properties of nanostructured bilayers (60-100 nm thickness with a ± 10 nm surface roughness) were calculated, keeping the interface between the layers as smooth flat surfaces. For the NbN/Nb nanostructure with a thickness between 100 ± 10 nm, and 70 ± 10 nm, in a wavelength range between 200 and 350 nm, the reflectance and absorptance show a nearly flat spectrum with an intensity of 20% and 80%, respectively. For larger wavelengths, absorptance decays smoothly. In contrast, for the 60 ± 10 nm bilayer, the absorptance decays faster. For the TiN/Ti nanostructure, at 415 nm, a relative maximum in the reflectance, and a minimum in absorptance, are observed. The critical value of the absorbed light spectra begins to shift to higher wavelengths as the thickness of the TiN layer increases. We demonstrate that adding a rough nitride layer on top of its metallized layer drastically modifies the optical response of the nanostructured bilayer, an interesting result for plasmonics and nanoelectronics applications.

Introduction




The development of nanostructured materials with physical properties that can be tailored has attracted great interest in recent decades. These materials promise potential applications for current technological devices. Particular interest has been focused in understanding the impact of nanoscaling the physical and chemical properties of both thin films and nanoparticles [1-4].

Morphology and roughness of thin films are some of the characteristics that can be explored to control the macroscopic electrical and optical properties of the films [4,5]. However, the effect of the roughness alone on the optical properties of thin films has been little studied. Both microstructural and optical properties seem to be highly dependent on the growth conditions utilized to prepare the films, such as working gas pressure, deposition rate, substrate temperature, and so on. On the other hand, in theoretical studies, it has been proposed to incorporate root mean square surface roughness into the models to better describe the dependence of the electrical resistivity on the roughness of ultrathin metal films at cryogenic temperatures [1,5,6]. Quantitative experimental data on the roughness in ultrathin films (<10 nm), as well as detailed studies of the dielectric function, however, are scarce and limited for the materials proposed in our study.


Nanostructured materials are now being studied in plasmonics. The field of plasmonics is of emerging interest due to the numerous real or potentially valuable applications of plasmon resonances in different materials, either in nanoparticles or in thin film form [7-9]. These applications vary from spectral coatings for chemical or biological sensors, medical diagnostic and therapeutic applications, to hybrid optoelectronic devices. Most of this research has been focused on gold and silver plasmonic nanostructures [10]. One of the most studied nanostructures are silver nanospheres, which exhibit a very strong plasmonic resonance in the blue end of the visible spectrum. Unfortunately, these nanostructures are susceptible to detrimental oxidation over several days [10-12].

Niobium, titanium, and their nitrides have been proposed as alternative plasmonic materials. They have superior advantages on gold or silver. For example, Nb maintains its bulk dielectric function even in ultrathin film form [13]. Furthermore, Nb has been proposed as a component in sensors and biosensors because its null degradation in aqueous solution. It is also a promising material in optoelectronic applications.

In this work, we model the optical response alteration caused by a surface roughness in mono and bilayers of Ni, Ti, and their nitrides. Reflectance (R), transmittance (T), and absorptance (A) of thin films with either smooth or rough surfaces were calculated by using the Discrete Dipole Approximation (DDA) model. Realistic surface-roughness patterns were incorporated into the model. The optical response in the visible range was analyzed for different thin film thicknesses. We demonstrate that in the case of a 60 ± 10 nm NbN/Nb bilayer with a rough surface, the absorptance decays more rapidly than in the other bilayers. On the other hand, in a TiN/Ti nanostructure, we demonstrate that the relative maximum commonly emerged in its absorptance spectra, initially at 415 nm, experiences an interesting red shift as the thickness of the TiN layer increases. This study can serve as a guide to experimental researches to fabricate this kind of nanostructured materials that may find a place in plasmonic and nanoelectronics applications.

J. Alberto Polito-Lucas , Valentin Garcia-Vazquez ,
[Ana L. González](#) 

*Instituto de Física, Benemérita Universidad Autónoma de Puebla
 Puebla, Pue. 72570, México.*

Francisco Javier Flores-Ruiz 
 CONAHCYT-Instituto de Física, BUAP
 Puebla, Pue. 72570, México.

Received: September 30th, 2023

Accepted: February 2nd, 2024

Published: February 19th, 2024

© 2024 by the authors. Creative Commons Attribution

https://doi.org/10.47566/2024_syv37_1-240201

Methodology

Simulating optical properties of films with a rough surface

Reflected, transmitted and absorbed light by thin films with either smooth or rough surfaces were determined by numerical simulations using the DDA model implemented in the DDSCAT code [14, 15]. With DDA, it is possible to study bidimensional nanostructures by making use of the well-known concept of unit cell utilized in solid state physics. In DDA, a target unit cell (TUC) is a unit block conveniently constructed and reproduced periodically in a plane in order to mimic the thin film by a set of point electric dipoles. Figure 1 shows the TUC chosen to mimic a bilayer composed by two smooth flat layers of generic materials *a* and *b*. With N_a and N_b as integer numbers, the TUC in the figure is a column composed by N_a and N_b point dipoles separated by a distance d_{dip} . Each point dipole is represented by a sphere in the figure. In order to resemble a solid thin film, the chosen TUC is replicated along the *YZ* plane with a periodicity $L_y = L_z = d_{dip}$.

Fundamentals of DDA are extensively detailed in [14], next, we give the general details. Each dipole is labeled at a position $\mathbf{r}_{j,mn}$, where *j* indicates the *j*-th dipole into the replica that is located *m* units along *y*-direction and *n* units along the *z*-direction. Each dipole moment in the TUC is given by

$$\mathbf{P}_{j,00} = \alpha_j [\mathbf{E}_{inc}(\mathbf{r}_{j,00}) - \sum_{k \neq j} \tilde{A}_{j,k} \mathbf{P}_{k,00}],$$

where α_j is the polarizability, \mathbf{E}_{inc} is the electric field evaluated at $\mathbf{r}_{j,00}$, $\tilde{A}_{j,k}$ is the interaction matrix among the dipole $\mathbf{r}_{j,00}$ and the electric field induced by the other dipoles of the TUC, as well as by the dipole $\mathbf{r}_{k,mn}$ of each replica. The total electric field at each position is given by the sum of the incident planewave field and the scattered field by the other dipoles. The scattered electric field can be calculated by the following expression:

$$\mathbf{E}_s = \frac{2\pi i \exp(i\mathbf{k}_s \cdot \mathbf{r} - i\omega t)}{k_0^2 A_{TUC} \sin \alpha_s} \mathbf{F}_{TUC}(\hat{\mathbf{k}}_s),$$

where $\hat{\mathbf{k}}_s$ is the scattered unit wavevector, α_s is the scattered wave angle and \mathbf{F}_{TUC} is a factor depending on $\hat{\mathbf{k}}_s$, incidence direction ($\hat{\mathbf{k}}_0$) and incident polarization state (\mathbf{E}_0). For a detail derivation of the latter equation, see [14]. Once the scattered field is known, it is possible to determine the elements S_i of the amplitude scattering matrix. For $\hat{\mathbf{k}}_s \neq \hat{\mathbf{k}}_0$, the matrix is related to the incident and scattered electric field:

$$\begin{bmatrix} \mathbf{E}_s \cdot \hat{e}_{s\parallel} \\ \mathbf{E}_s \cdot \hat{e}_{s\perp} \end{bmatrix} = i \exp(i\mathbf{k}_s \cdot \mathbf{r} - i\omega t) \begin{bmatrix} S_2 & S_3 \\ S_4 & S_1 \end{bmatrix} \begin{bmatrix} \mathbf{E}_0 \cdot \hat{e}_{i\parallel} \\ \mathbf{E}_0 \cdot \hat{e}_{i\perp} \end{bmatrix},$$

where $\hat{e}_{s\parallel}$, $\hat{e}_{s\perp}$, $\hat{e}_{i\parallel}$ and $\hat{e}_{i\perp}$ the scattered and incident unit polarization vectors parallel and perpendicular to the scattering plane. In addition, the properties of the far-field scattering of an isolated target are determined by the 4×4 Mueller matrix ($S_{\alpha\beta}$), which is dimensionless. The Mueller matrix elements $S_{\alpha\beta}$ can be expressed in terms of the amplitude scattering matrix elements S_i (see reference [16]

for the explicit expressions). The Stokes vectors of the incident and scattered electric polarization states are related by the next expression:

$$\begin{pmatrix} I_s \\ Q_s \\ U_s \\ V_s \end{pmatrix} = \frac{1}{k^2 r^2} \begin{pmatrix} S_{11} & S_{12} & S_{13} & S_{14} \\ S_{21} & S_{22} & S_{23} & S_{24} \\ S_{31} & S_{32} & S_{33} & S_{34} \\ S_{41} & S_{42} & S_{43} & S_{44} \end{pmatrix} \begin{pmatrix} I_i \\ Q_i \\ U_i \\ V_i \end{pmatrix},$$

where I_s , Q_s , U_s , V_s , I_i , Q_i , U_i and V_i are the Stokes vector components. Finally, the reflected (*R*), and transmitted (*T*) light is obtained from [14, 16]:

$$R_{\parallel} = S_{11}(k_{sx} = -k_{0x}) + S_{12}(k_{sx} = k_{0x}),$$

$$R_{\perp} = S_{11}(k_{sx} = -k_{0x}) - S_{12}(k_{sx} = k_{0x}),$$

$$T_{\parallel} = S_{11}(k_{sx} = k_{0x}) + S_{12}(k_{sx} = k_{0x}),$$

and

$$T_{\perp} = S_{11}(k_{sx} = k_{0x}) - S_{12}(k_{sx} = k_{0x}),$$

where R_{\parallel} , R_{\perp} , T_{\parallel} , and T_{\perp} , are the reflection and transmission coefficients, respectively, parallel and perpendicular to the plain defined by the surface normal and $\hat{\mathbf{k}}$.

We used the DDSCAT v7.3.1 code to calculate the far-field optical response of the thin films. The code calculates the scattered field of the dipole array, the elements of the Mueller matrix, and the *R* and *T* coefficients, among other

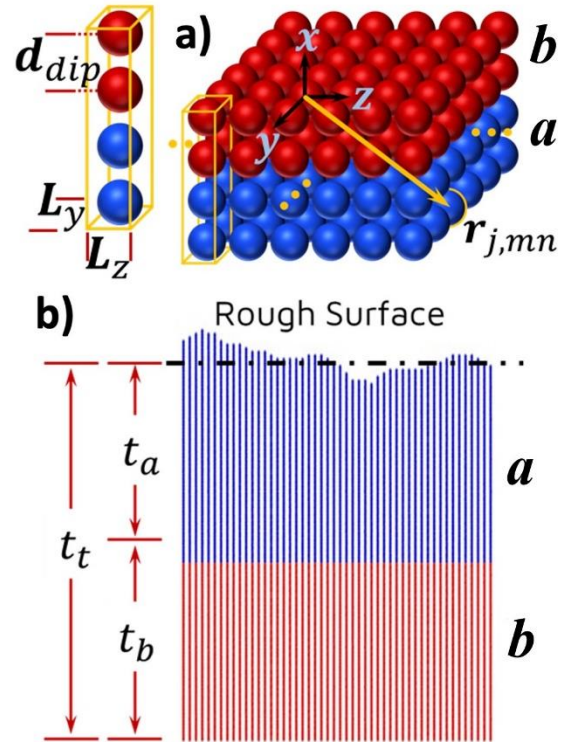


Figure 1. a) Left: Schematic representation of a TUC composed by two generic material *a*; red spheres, of a generic material *b*. Right: Multiple replicas of the TUC representing an infinite thin film with a bilayer *a/b* structure and having a smooth flat surface. Incident light strikes first on layer *a*. b) Cross section of a TUC to mimic an *a/b* bilayer with rough surface. The red dots represent the smooth layer with thickness t_b . The blue dots represent the layer with roughness and thickness t_a .

physical quantities. The absorbance is simply obtained from $A = 1 - R - T$. For the point dipoles that represent the layer a , the dielectric function of material a is assigned; for those of layer b , the dielectric function of material b . In this work, we used the dielectric function of Nb and Ti reported from bulk materials in references [17] and [18], respectively. Whereas for NbN and TiN, we used those values reported from stoichiometric samples with a nitrogen concentration percentage of $50\% \pm 0.5\%$ [19]. We assume the air as the surrounding medium. Substrate was not taken into account in our numerical simulations. A planewave with normal incidence and two possible linear polarization states impact first on the layer a and then transmits to the layer b .

In order to explore the effect of the roughness on the surface of a bilayer structure, we limit to the case where the layer b and the $a - b$ interface are both smooth, whereas the interface of the layer a with the air is the only that is rough (see Figure 1c). With the notation a/b we indicate that the light comes in through the layer a and goes out from layer b . The thickness of layer a is denoted with t_a and that of layer b is denoted with t_b . In order to perform numerical simulations of a surface with realistic roughness, we used a roughness pattern experimentally obtained from a Nb thin film deposited on Si <100> substrate by magnetron DC sputtering. Details are explained in the next section.

After a preliminary study of convergence, we found that d_{dip} must be of the order of 3.5 nm for layers that have a thickness between 100 and 50 nm. In this study, we modeled nanostructured bilayers with thickness 100, 80, 70 and 60 nm. For the surface roughness, we used a value of ± 10 nm.

Results and discussion

A thin film of Nb was deposited by magnetron DC sputtering using a Si <100> substrate. Table 1 shows the experimental parameters used during deposition. Figures 2a and 2b show the experimental spectra (solid lines) obtained for this sample for p-(parallel) and s-(perpendicular) reflectance respectively, obtained at different angles of the incident light. These experimental results were compared to those obtained with DDA (dashed lines) considering the same thickness of the actual sample but with a smooth surface. The calculated and measured spectra show the same shape-line but slightly different intensities. The numerical calculations were performed considering a smooth surface and using a dielectric function of a bulk sample (without border grains). The latter explains the prediction of a higher reflectivity than that measured for the Nb thin film. The topography of the obtained film was measured with a Bruker Dimension Edge atomic force microscope (AFM) in ScanAsyst measurement mode. A ScanAsyst Contact Air probe with a tip radius of curvature <20 nm was used. The film is 100 nm thick, and has a roughness of ± 1 nm. Figure 2c shows a representative AFM image of the sample. A uniform distribution of particles and thickness of the thin film was observed along the sample.

To perform numerical simulations of a rough surface, an actual roughness pattern was obtained from the AFM image

Table 1. Parameters used during the deposition of Niobium thin film by magnetron sputtering DC.

Parameter	Niobium
Material	Niobium
Substrate	Single-crystalline silicon <100>
Pre-Sputtering time	10 minutes at 100 watts DC
Substrate temperature	Room temperature (293 K)
Ar plasma pressure	4.8 ± 0.1 mTorr
Power	200 watts DC
Deposition time	3.5 minutes

of Nb thin film (Figure 2c). The entire AFM image has a size of $1 \mu\text{m}^2$ and 512p. The AFM equipment provides a file with the coordinates of the sample and the measured heights, these data were processed and we extracted only those of the zone A. The area A has a size of $2.5 \times 10^{-3} \mu\text{m}^2$, due to the computational limitations, we created a TUC from this small square area, but this area is sufficient to reproduce the uniform rough surface (results not shown here). The extracted data were then used as the dipole coordinates of the TUC. Figure 2d shows a schematic representation of the TUC's surface and its replicas along the y-z plane with a periodicity of $L_y = L_z = 50$ nm. Each point dipole of the TUC is represented by a blue dot. Notice that only the dipoles of the TUC's surface are shown; the rest of dipoles composing the thick of the film are not illustrated for an easy view. The dashed red lines in the figure are just a guide to the eye to permit identify the replications of the TUC. In the calculations, however, the TUC and its replicas are next to each other, creating an infinite continuous rough surface. Figures 3a and 3b show the calculated reflected, transmitted, and absorbed light obtained for ideal smooth layers of Nb and NbN, respectively. The thickness of each layer is 50 nm. At normal incidence and above 200 nm, the light on the Nb

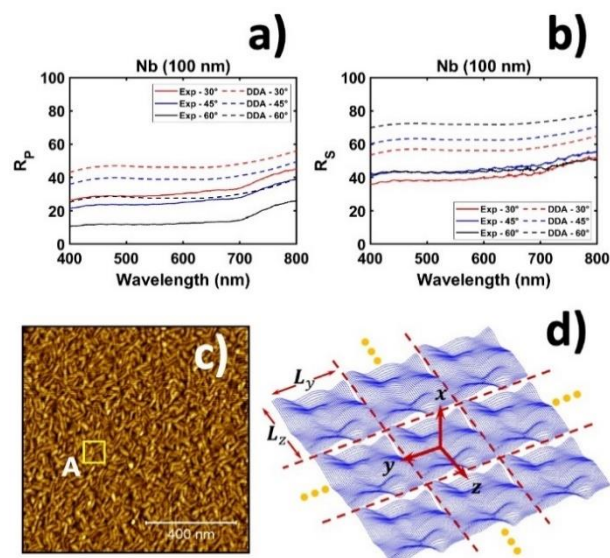


Figure 2. a) Parallel and b) Perpendicular reflected light of a 100 nm thick Nb film (dashed lines are calculated and solid lines are experimental). c) AFM image of the Nb thin film. Zone A, marked with a yellow square, was chosen to create a TUC. d) Schematic representation of the TUC's surface and its replicas along the y-z plane mimicking a thin film with a roughened surface. Each point dipole of the TUC is represented by blue dots. Only the surface of the TUC is shown for illustration purposes.

metallic layer is mostly reflected and absorbed, whereas a relatively insignificant amount is transmitted. The transmitted light by the NbN layer is also insignificant compared to the reflected and absorbed light. Figures 3c and 3d show R, T and A of a bilayer of Nb and NbN with a configuration a/b , indicating that the light travels from layer

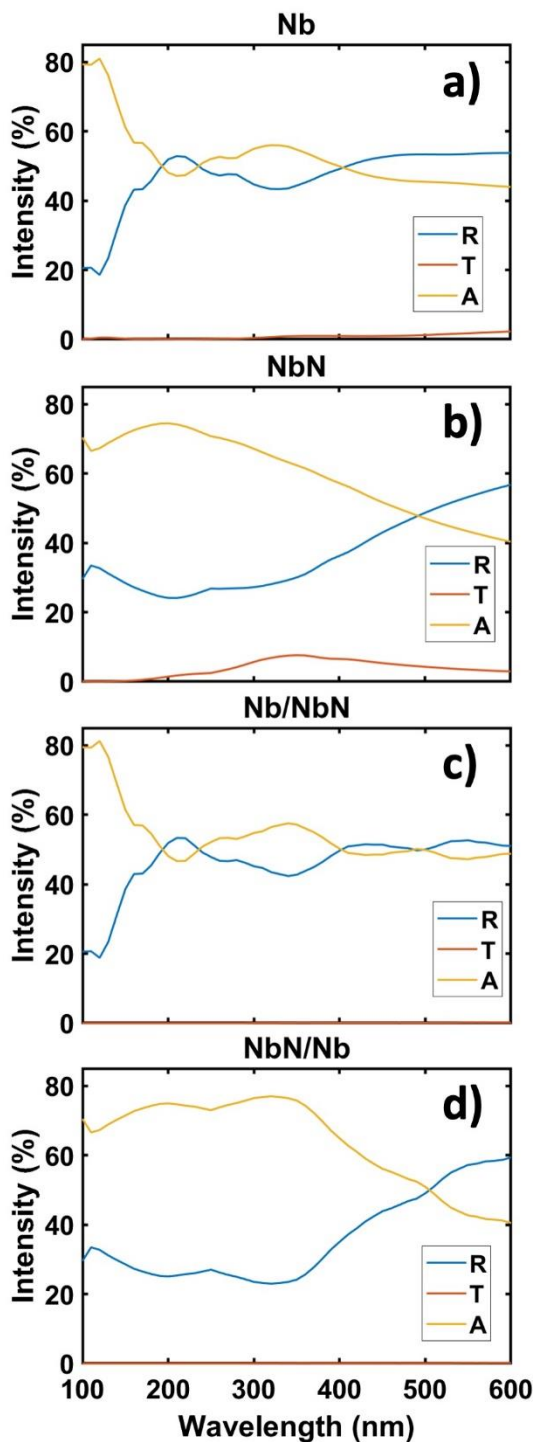


Figure 3. Reflected (R), transmitted (T) and absorbed (A) light of layers at normal incidence. In a) and b) R, T y A are shown for ideal smooth monolayers of Nb and NbN, respectively. Each layer has a thickness of 50 nm. In c) and d), is shown the response of an ideally smooth (zero roughness) bilayer of materials a/b with total thickness $t_t = 100$ nm and $t_a = t_b = 50$ nm. The incident light travels from layer a through layer b .

a through layer b . The thickness of each layer is of 50 nm, and the total bilayer thickness is, therefore, 100 nm. We observe that, from Figure 3c, that in an interval of wavelengths from ultraviolet to visible, the optical response of the Nb/NbN bilayer is similar to that of a single Nb layer, except at wavelengths of 400 nm and larger. This indicates that at those wavelengths, the small portion of light that gets transmitted by the Nb layer is enough to excite the adjacent NbN layer.

When Nb and NbN layers are interchanged in the bilayer, *i.e.*, when the light travels from the NbN layer to the Nb layer, the response changes, see Figure 3d. An optical band at 320 nm is then observed in the reflectance and absorptance spectra, a consequence of a maximum that is observed in transmittance. Considering these results, we follow by exploring further the optical response of bilayer structures where NbN and TiN play the role of layer a .

Reflectance and absorptance spectra of NbN/Nb bilayer structures are shown in Figure 4. Here, the air-NbN interface is rough, whereas the NbN-Nb interface remains smooth. In these spectra, the thickness t_a of the Nb layer was fixed at 50 nm, the thickness t_b of the NbN layer was varied from 50 nm to 10 nm, and a roughness of ± 10 nm was utilized. Total thickness of these bilayers, therefore, was varied from 100 ± 10 nm to 60 ± 10 nm. In the reflectance spectrum of the bilayer with a rough surface, we observe a decrease in intensity of about 10%. We visualize that the bands observed at 250 and 320 nm for the smooth bilayer are smoothed and form a flat spectrum with 20% of reflection for the bilayers with rough surfaces and thicknesses of 100, 80, and 70 ± 10 nm. In the case of the 60 ± 10 nm bilayer, we can

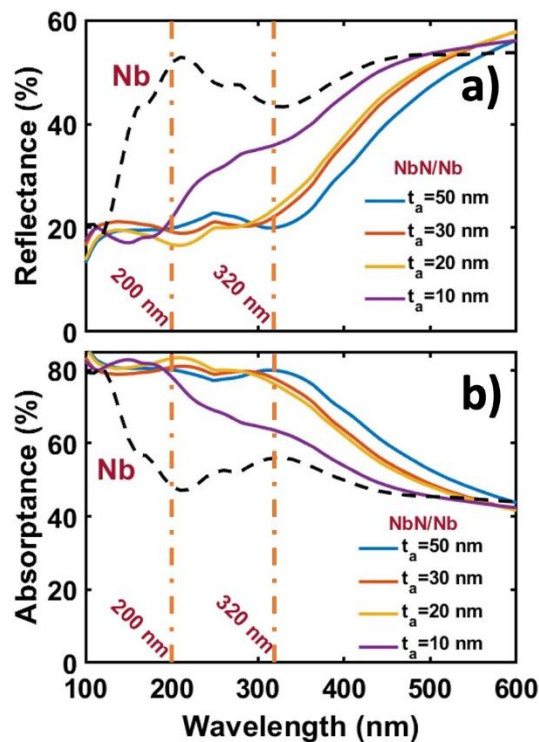


Figure 4. Reflectance (a) and absorptance (b) spectra of a NbN/Nb bilayer (NbN as layer a) with a NbN rough surface (see illustration in Figure 1b). The t_a thickness is varied from 10 to 50 nm with a roughness of ± 10 nm.

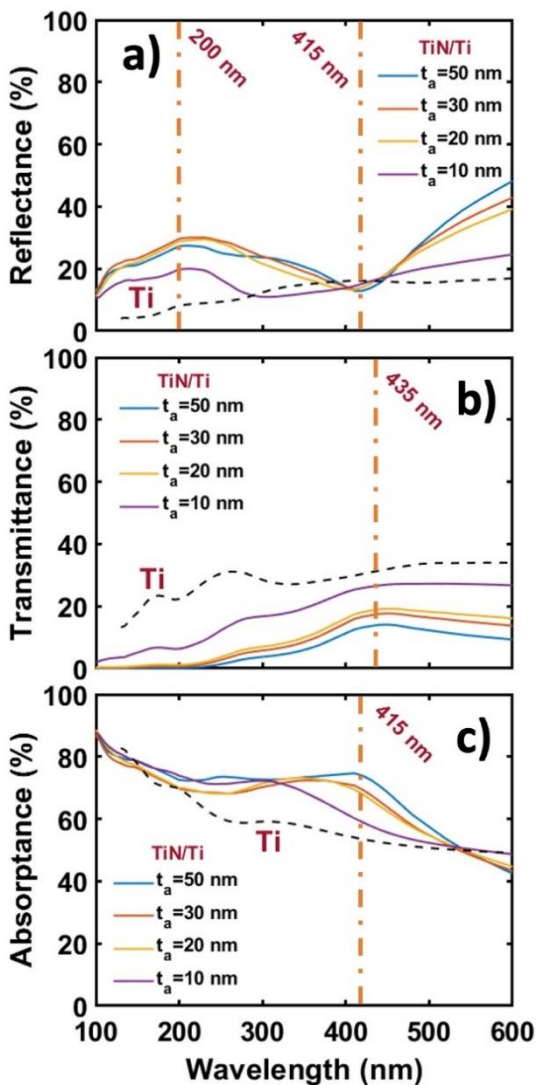


Figure 5. Reflectance (a), transmittance (b) and absorbance (c) spectra of a TiN/Ti bilayer varying the thickness of the TiN layer from 10 to 50 nm with a roughness of ± 10 nm. The thickness of Ti layer remains constant at 50 nm.

notice a relative minimum at 150 nm, followed by an increase as the wavelength increases.

The same behavior is observed in the absorbed light spectra of the NbN/Nb bilayer with a rough surface. For the thicknesses of 100 ± 10 , 80 ± 10 , and 70 ± 10 nm, 80% of light is absorbed by the bilayers when the incident wavelength is in the range of 100 to 350 nm. For larger wavelengths, the absorption decays smoothly. On the other hand, for the 60 ± 10 nm bilayer with a rough surface, the absorbance decays faster than the one observed in the other bilayers. These behaviors, both in the reflectance and the absorbance, of the 60 ± 10 nm bilayer with a rough surface is due to the decrease in the thickness of the NbN layer. This decrease in thickness implies that the incident light is transmitted in greater amounts towards the Nb layer that composes the nanostructure.

Finally, for the TiN/Ti nanostructured material, its optical response spectra are shown in Figure 5. In the reflectance spectrum, a relative maximum at 220 nm and minimum at

415 nm are visualized. The same behavior is observed in the TiN/Ti [$t_a=50$ nm] and TiN/Ti [$t_a=20$ nm] nanostructures. In the case of TiN/Ti [$t_a=10$ nm], the maximum is observed at 220 nm, whereas above 300 nm the qualitative behavior resembles that of a Ti monolayer. In its transmittance spectrum, a decrease in the intensity is observed as the thickness of the TiN layer begins to increase. In addition, a band at 435 nm begins to slightly define. On the other hand, in the absorbance spectrum, a relative maximum at 415 nm is observed. It should be noted that this maximum begins to shift towards longer wavelengths, *i.e.*, at lower energies, as the thickness of the TiN layer with a rough surface increases.

Conclusions

We performed numerical calculations of the reflected, transmitted, and absorbed light by mono and bilayers of Niobium, Titanium and their nitrides. Calculations were carried out on both smooth films and films with a rough surface. We have demonstrated that the thickness and the surface roughness of the studied nanostructures play an important role on their optical properties. In a smooth bilayer of Nb/NbN, when the light impinges normally and travels from the Nb layer through the NbN layer, the optical response is similar to that of a single Nb layer, except at wavelengths of 400 nm and larger. Above 400 nm, the small amount of light transmitted by the Nb layer is sufficient enough to excite the adjacent NbN layer. Contrasted changes are observed in R and T when the light travels in the opposite direction. For a bilayer of NbN/Nb with rough surface and total thickness of 100 ± 10 nm to 70 ± 10 nm, the reflectance (20%) and absorbance (80%) are practically flat in a wavelength range between 200 and 350 nm. As a general trend, the absorbed light decreases smoothly as the wavelengths increase. In the case of TiN/Ti nanostructure, an absorption band is detected around 415 nm. It shifts to higher wavelengths as the thickness of the TiN layer increases.

Furthermore, we have also demonstrated that a rough nitride layer on top of its metallized layer is able to tune the optical bands of the second one, a significant result that could be used in multiple applications, mainly in plasmonics and nanoelectronics.

Acknowledgements

Authors thank VIEP BUAP for the grant to projects 100504244-VIEP2023 and 100187688-VIEP2023. F. Flores also thanks CONAHCYT for supporting the CF-2023-I-1429 project. J. A. Polito Lucas acknowledges CONAHCYT for the scholarship #861219.

References

- [1]. D. Josell, S.H. Brongersma, Z. Tökei, *Annu. Rev. Mater. Res.* **39**, 231 (2009).
- [2]. M.N. Esfahani, B.E. Alaca, *Adv. Eng. Mater.* **21**, 1900192 (2019).
- [3]. P. Bhagowati, P. Saha, M.B. Sahariah, *Comp. Mat. Sc.* **220**, 112060 (2023).
- [4]. A. Amirjani, N.N. Koochak, D.F. Haghshenas, *J. Chem. Educ.*

[96, 2584 \(2019\)](#).

[5]. Y.P. Timalisina, A. Horning, R.F. Spivey, K.M. Lewis, T.S. Kuan, G.C. Wang, T.M. Lu, [Nanotechnology 26, 075704 \(2015\)](#).

[6]. S. Chatterjee, A.E. Meyerovich, [Phys. Rev. B 81, 245409 \(2010\)](#).

[7]. H. Reddy, U. Guler, Z. Kudyshev, A.V. Kildishev, V.M. Shalaev, A. Boltasseva, [ACS photonics 4, 1413 \(2017\)](#).

[8]. C. Gao, Y. Hu, M. Wang, M. Chi, Y. Yin, [J. Am. Chem. Soc. 136, 7474 \(2014\)](#).

[9]. S. Liu, G. Chen, P.N. Prasad, M.T. Swihart, [Chem. Mater. 23, 4098 \(2011\)](#).

[10]. K. Khurana, N. Jaggi, [Plasmonics 16, 981 \(2021\)](#).

[11]. U. Guler, R. Turan, [Opt. Express 18, 17322 \(2010\)](#).

[12]. Y. Cai, Y. Li, P. Nordlander, P.S. Cremer, [Nano Lett. 12, 4881 \(2012\)](#).

[13]. G.V. Naik, V.M. Shalaev, A. Boltasseva, [Adv. Mat. 25, 3264 \(2013\)](#).

[14]. B.T. Draine, P.J. Flatau, [J. Opt. Soc. Am. A 25, 2693 \(2008\)](#).

[15]. B.T. Draine, J.C. Weingartner, [Astrophys. J. 480, 633 \(1997\)](#).

[16]. C.F. Bohren, D.R. Huffman, [Absorption and scattering of light by small particles \(WILEY-VCH, 2008\)](#).

[17]. J.H. Weaver, D.W. Lynch, C.G. Olson, [Phys. Rev. B 7, 4311 \(1973\)](#).

[18]. D. Barchiesi, T. Grosjes, [J. Nanophotonics 8, 083097 \(2014\)](#).

[19]. H.A. Wriedt, J.L. Murray, [Bull. Alloy Phase Diagr. 8, 378 \(1987\)](#).

© 2024 by the authors; licensee SMCTSM, Mexico. This article is an open access article distributed under the terms and conditions of the Creative Commons Attribution license (<http://creativecommons.org/licenses/by/4.0/>).